ORIGINAL PAPER

Enhanced the electrochemical performances of LiNi$_{0.7}$Co$_{0.15}$Mn$_{0.15}$O$_2$ cathodes by the hybrid ZrO$_2$-Li$_2$ZrO$_3$ layer

Wei Li [1,2,3] · Yunjiao Li [1,2,3] · LiShan Yang [4] · Jie Zhu [1,2,3] · Jia Guo [1,2,3] · Jia Chao Yang [1,2,3]

Abstract

Electrode-electrolyte interface side reactions cause the fast capacity fading of Ni-rich cathode, especially at high cutoff voltages and high temperatures. This is the main obstacle for their commercial application. Herein, a hybrid ZrO$_2$-Li$_2$ZrO$_3$ (LZO) coating layer was fabricated through a wet process on LiNi$_{0.7}$Co$_{0.15}$Mn$_{0.15}$O$_2$ (NCM) cathode materials. The structure and chemical composition of the ZrO$_2$-Li$_2$ZrO$_3$ coating layer were studied by the characterizations of XRD, SEM, TEM, and XPS. The ZrO$_2$-Li$_2$ZrO$_3$-coated LiNi$_{0.7}$Co$_{0.15}$Mn$_{0.15}$O$_2$ cathode improved cycling stabilities at both 25 and 55 °C in the case of high cutoff voltage. In detail, ZrO$_2$-Li$_2$ZrO$_3$-coated NCM (LZO-NCM) delivers a 187.40 mAh g^{-1} with 83.4% capacity retention after 100 cycles at 1C over 3.0–4.5 V, and it is far higher than that of uncoated sample (71.4%). At elevated temperature (55 °C), the ZrO$_2$-Li$_2$ZrO$_3$-coated sample also maintains 79% capacity retention after 100 cycles (3.0–4.5 V, 1C), which is higher than the 61.5% capacity retention of the pristine electrode. The hybrid ZrO$_2$-Li$_2$ZrO$_3$ coating could not only keep the bulk structure stability but also prevent the electrochemical resistance which varies after cycles. Thereby, the electrochemical properties were improved significantly.

Keywords LiNi$_{0.7}$Co$_{0.15}$Mn$_{0.15}$O$_2$ · ZrO$_2$-Li$_2$ZrO$_3$ coating layer · Side reaction · High voltage · High temperature

Introduction

In the past decades, lithium-ion batteries (LIBs) have been rapidly developed and applied in most fields, especially in electric vehicles [1–4]. LIBs with high energy density are of significance in EVs to meet the requirement of longer endurance mileage [5, 6]. One of the most important factors affecting the LIB energy density is the cathode material, among which the Ni-rich cathodes have attracted much attention because of its relatively high capacity [7–10]. Generally, the increase of capacity can be achieved by increasing the nickel content in Ni-rich cathodes and/or enhancing the cutoff voltage [11–15].

However, Ni-rich cathodes such as LiNi$_{0.7}$Co$_{0.15}$Mn$_{0.15}$O$_2$ and LiNi$_{0.8}$Co$_{0.1}$Mn$_{0.1}$O$_2$ have so far been retarded by electrode-electrolyte interface side

✉ Yunjiao Li
yunjiao_li@csu.edu.cn

Wei Li
35251011@qq.com

LiShan Yang
Yang@hunnu.edu.cn

Jie Zhu
361281832@qq.com

Jia Guo
397115643@qq.com

Jia Chao Yang
904025697@qq.com

1 School of Metallurgy and Environment, Central South University, Changsha 410083, People's Republic of China

2 Engineering Research Center of the Ministry of Education for Advanced Battery Materials, Central South University, Changsha 410083, People's Republic of China

3 Changsha Research Institute of Mining and Metallurgy, Changsha 410083, People's Republic of China

4 National & Local Joint Engineering Laboratory for New Petrochemical Materials & Fine Utilization of Resources, Key Laboratory of Chemical Biology and Traditional Chinese Medicine Research (Ministry of Education of China), Key Laboratory of the Assembly and Application of Organic Functional Molecules of Hunan Province, Hunan Normal University, Changsha 410081, People's Republic of China

reactions, which leads to the low capacity retention with dramatic voltage plateau dropping, especially at high cut-off voltages and high temperatures [16–19]. In the higher voltage charging state, the highly oxidized and active Ni^{4+} on the surface of the material is prone to interface side reaction with electrolyte, leading to the surface structure instability of the cathode materials due to the irreversible phase transition on the surface [20–22]. In addition, the residual lithium on the particle surface of Ni-rich cathode materials can bring out more dissolution of the transition metals from the particle surface, leading to the capacity fading [23, 24]. Another problem with Ni-rich cathode materials is related to structural instability in high temperature. Transition metal ions dissolving into the electrolytes in high temperature aggravated the partial phase transformation to spinel phase, which decreases the safety performances [25, 26].

Surface coating has been proved to be one of the effective methods to solve some of the above problems [27–31]. By providing a shield at the material surface, the electrode surface is protected from reacting with the electrolyte, and the side reactions between the cathode and the electrolyte are prohibited so as to improve the electrochemical performances of the Ni-rich cathode materials [32–35]. The metal oxides and fast ion conductors have been developed as promising coatings. Metal oxides can be used as the HF scavenger in electrolyte, which protects the positive electrode material from HF corrosion and inhibits further decomposition of the electrolyte [32, 36]. The fast ionic conductors can improve the electrochemical performance by increasing the electrical conductivity [11, 37, 38]. In combination with the characteristics of the two cladding materials, in this paper, ZrO_2-Li_2ZrO_3 (mark as LZO) multiphase layer was used to coat $LiNi_{0.7}Co_{0.15}Mn_{0.15}O_2$ via a wet process, and the effects of the LZO coating layer on $LiNi_{0.7}Co_{0.15}Mn_{0.15}O_2$ were systematically discussed. Furthermore, the electrochemical performance of prepared powder as cathodes was evaluated at both the room temperature and a higher temperature.

Experimental

Synthesis of $LiNi_{0.7}Mn_{0.15}Co_{0.15}O_2$

For the preparation of pristine $LiNi_{0.7}Co_{0.15}Mn_{0.15}O_2$ materials, commercial $Ni_{0.7}Co_{0.15}Mn_{0.15}(OH)_2$ (Hunan Brunep Recycling Corp., China) precursor was mixed thoroughly with $LiOH \cdot H_2O$ ($n_{Li}/n_{(Ni + Co + Mn)} = 1.04$) and sintered at 820 °C in O_2 flow for 10 h. Then, the pristine $LiNi_{0.7}Mn_{0.15}Co_{0.15}O_2$ materials (mark as NCM) were prepared.

Synthesis of ZrO_2-Li_2ZrO_3-coated $LiNi_{0.7}Mn_{0.15}Co_{0.15}O_2$

LZO-coated $LiNi_{0.7}Co_{0.15}Mn_{0.15}O_2$ (LZO-NCM) materials were synthesized in the following procedure showed in Fig. 1. A total of 200 g $LiNi_{0.7}Co_{0.15}Mn_{0.15}O_2$ powders was dispersed into 200 ml $Zr(CH_3COO)_4$ (~ 1.07 g) aqueous solution and stirred for 2 min to achieve good dispersion, and then $NH_3 \cdot H_2O$ aqueous solution was slowly added into the above suspension to produce a slurry. Then, the slurry was dried at 60 °C in a vacuum oven. Lastly, the obtained solid was calcined at 600 °C in O_2 flow for 6 h to obtain the final products. Based on the ICP-OES test, it can be considered that the mass ratio of ZrO_2 (here, we assume that all Zr are in the state of ZrO_2) to $LiNi_{0.7}Co_{0.15}Mn_{0.15}O_2$ is about 0.2 wt%.

Physical characterization

X-Ray diffraction (XRD, Panaco X Pert PRO) with a Cu K_{α} radiation source was employed to identify the crystalline structures of the samples. The scanning rate was 8°/min. Particle morphology and elemental mapping of the prepared powders were observed by scanning electron microscopy (SEM, Hitachi S3400N, Japan), and the status of the coating layers of the samples was studied by transmission electron microscopy (TEM, Tecnai G12, 200 kV). X-Ray photoelectron spectroscopy (XPS, VG Multilab 2000) measurements were performed to get information on the elements' composition on samples' surface. Cycled coin half cells were disassembled in the argon glove box (MNIUIVESAR1220-100, MIKROUNA) and the powder scraped from the obtained electrodes washed by dimethyl carbonate (DMC) for XRD analysis.

Electrochemical testing

CR2016-type coin button cells were assembled to perform the electrochemical characterizations. Positive electrodes were prepared by mixing the cathode powders with 10 wt% acetylene black and 10 wt% polyvinylidene fluoride (PVDF) binder in the proper amount of N-methyl-2-pyrrolidone (NMP). The blended slurries were cast onto an aluminum current collector and dried under vacuum at 120 °C for 12 h. CCR2016-type coin button cells were fabricated in the Ar-filled glovebox (MNIUIVESAR1220-100, MIKROUNA, China). We used lithium foil as the negative electrode, Celgard 2400 as the separator, and 1 M $LiPF_6$ dissolved in the liquid of EMC:EC:DMC = 1:1:1 vol ratio as the electrolyte.

The initial charge/discharge cycle at 0.1C (1C = 180 mA g^{-1}) and the following cycle at 1C of the half cells were tested by Neware Test System (CT-4008-5V6A-S1, Shenzhen Neware Energy Tech Co., Ltd., China) at a voltage between 3.0 and 4.5 V at 25 °C and 55 °C. Cyclic

Fig. 1 Scheme illustrating the coating process from pristine NCM cathodes to ZrO$_2$-Li$_2$ZrO$_3$-coated NCM cathodes
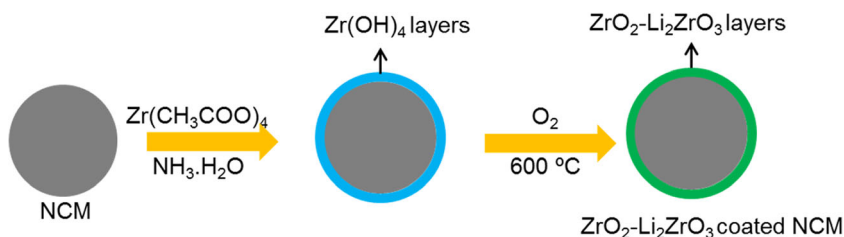
voltammetry (CV, 3.0–4.5 V, 0.1 mV s^{-1}) measurements were carried out on a CHI750E electrochemical workstation (CHI750E, Shanghai, China). After the first and 50th cycles, we performed electrochemical impedance spectra (EIS) of cells using CHI750E with an amplitude of 5 mV over a frequency range of 0.1 MHz to 10 mHz.

Results and discussion

In Fig. 2, the XRD patterns for NCM and LZO-NCM are well indexed to α-NaFeO$_2$ structure in a hexagonal form with $R\bar{3}m$ space group (JCPDS #09-0063) [38]. The slight shift to the lower angle for (003) peak of the LZO-NCM (Fig. 2b) indicates the possible phase variation on the surface structure as a result of a trace doping of Zr^{4+} ions into the NCM crystals [20]. The splitting peaks of (018)/(110) in Fig. 2c represent a well-ordered layered structure in both samples. The lattice parameters (c and a) of LZO-NCM are 14.2175 Å and 2.8714 Å, which are similar to those of the NCM sample (c = 14.2177 Å and a = 2.8715 Å). Such small changes reveal that the bulk structure of NCM is not affected by the LZO coating. As shown in Fig. 2d, weak ZrO$_2$ signals (JCPDS #49–1642) appear in the pattern of LZO-NCM in the angle range of 26 ~ 29° (2θ) while none is observed for pristine NCM.

Fig. 2 **a** XRD patterns of the NCM and LZO-NCM, and **b** the expanded view of the NCM (003), **c** NCM (018/110), and **d** coating layer reflections
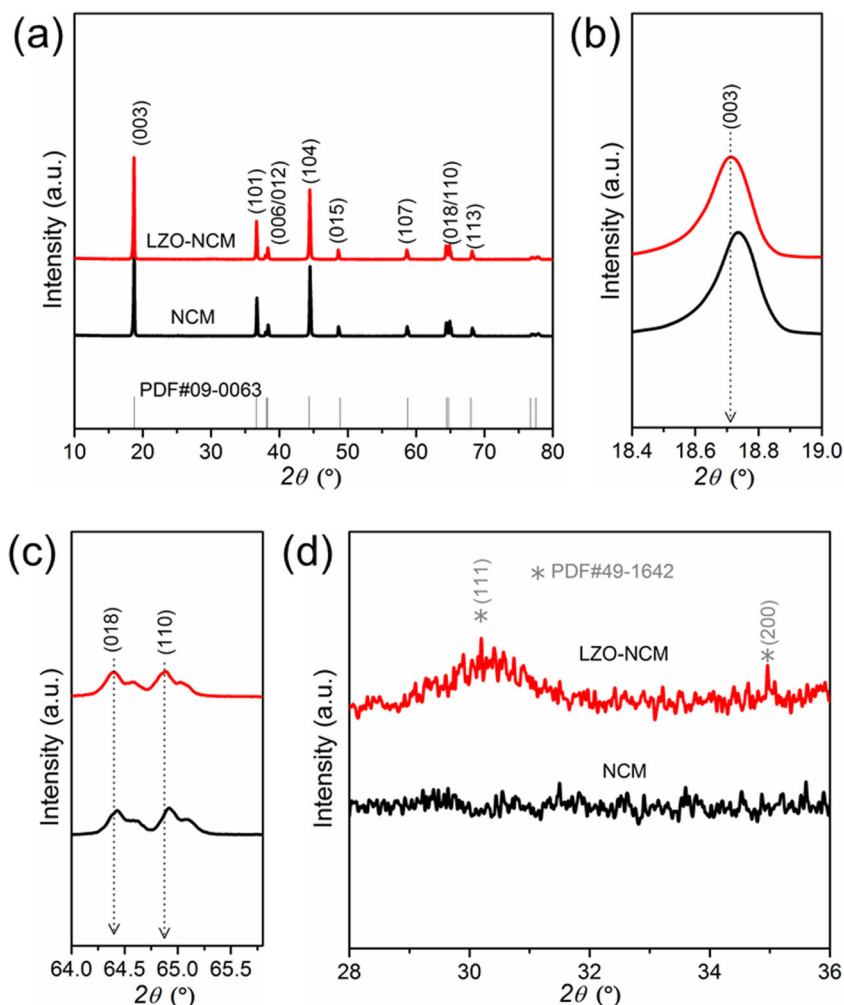
Figure 3a and d show the SEM images of NCM and LZO-NCM materials, in which all samples display spherical-like particles with about ~ 1 μm primary particles. The surface of coated samples (Fig. 3d) became obscure with some tiny nanoparticles while the particles of pristine NCM are clean and smooth. In more detail, the TEM images were used to characterize the structural characteristics of the samples. Compared with Fig. 3b and e, an ultra-thin coating layer can be clearly found on the particle surface after LZO modification. From the HRTEM images of pristine NCM (Fig. 3c), a layered crystal structure with a clear lattice fringe of ~ 0.479 nm agrees well with the distance of (0 0 3) crystal facet of the $LiNi_{0.7}Mn_{0.15}Co_{0.15}O_2$ (JCPDS #09-0063) [28]. In addition, the corresponding FFT pattern (inset in Fig. 3c) shows an array of hexagonal symmetry dots, and revealed the single crystalline feature of the NCM. Furthermore, the surface shows an amorphous layer, which associates with the surface lithium residual (Li_2CO_3/LiOH). In addition, some different lattice fringes with interplanar spacing of ~ 0.16 nm and ~ 0.296 nm are also observed near the NCM boundaries (Fig. 3f), along with the corresponding FFT pattern (inset in Fig. 3f), which corresponds to the (2 0 2) planes of Li_2ZrO_3 (JCPDS #41-0324) and (1 1 1) planes of ZrO_2 (JCPDS #49-1642), respectively. This demonstrates the existence of Li_2ZrO_3 and ZrO_2 on the surface of coated samples.

The energy-dispersive X-ray spectroscopy (EDS) mappings are present to check the element distribution of the LZO-NCM. Figure 4 indicates that the Zr elements are completely overlapped with Ni, Co, and Mn, suggesting that LZO coating layers were fully distributed throughout the NCM surface. This LZO multiphase coating layer is designed to act not only as a protection layer but also as an ion conductive layer, with possible effects on alleviating side reactions and improving the electrochemical performance of the $LiNi_{0.7}Mn_{0.15}Co_{0.15}O_2$, which would be discussed later.

XPS analysis was performed to find out the surface chemical compositions of pristine NCM and LZO-NCM. The survey spectra of both samples show typical Ni, Mn, and Co peaks, but Zr peaks are only observed in the LZO-NCM sample (Fig. 5a). The spectra of Ni 2p of both samples are shown in Fig. 5b. The Ni 2p binding energies show no obvious variations, suggesting that LZO coating does not affect the bulk cathode. This phenomenon is consistent with the results discussed in the previous XRD analysis. From Fig. 5c, the binding energy (BE) of Zr 3d at 182.2 eV and 184.7 eV is consistent with the reported value in ZrO_2 and Li_2ZrO_3 bulk material [39, 40]. Figure 5d exhibits the O 1s spectra of two samples. The BE located at 531.6 eV corresponds to the absorbed oxygen from surface lithium residual, while the small peak located at 529.8 eV is attributed to the oxygen in the metal framework [41]. As can be seen from Fig. 5d, compared with NCM, the O1s peak of LZO-NCM at 531.6 eV is slightly reduced than that of NCM, indicating that LZO coating may decrease amounts of the lithium residues, which may be favorable to improving the interfacial properties and leading to excellent electrochemical properties.

Figure 6 shows the initial charge/discharge curves at 0.1C and cycle performance at 1C of two samples between 3.0 and 4.5 V at 25 °C and 55 °C. As can be seen from Fig. 6a, the initial discharge capacities and corresponding coulombic efficiencies of two samples are 200.2 mAh g^{-1}/89.14% (NCM) and 196.3 mA h g^{-1}/89.57% (LZO-NCM), respectively. The
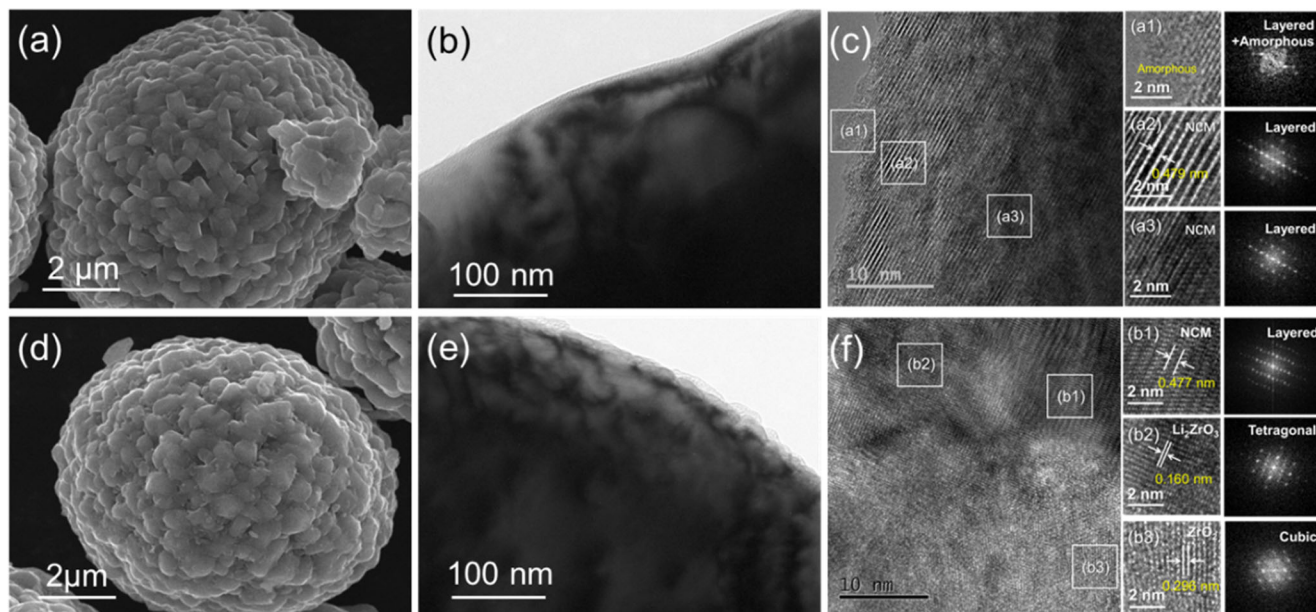
Fig. 3 SEM images for a NCM and d LZO-NCM spherical materials. TEM images for b NCM and e LZO-NCM. High-resolution (HRTEM) images for the c NCM and f LZO-NCM cathodes
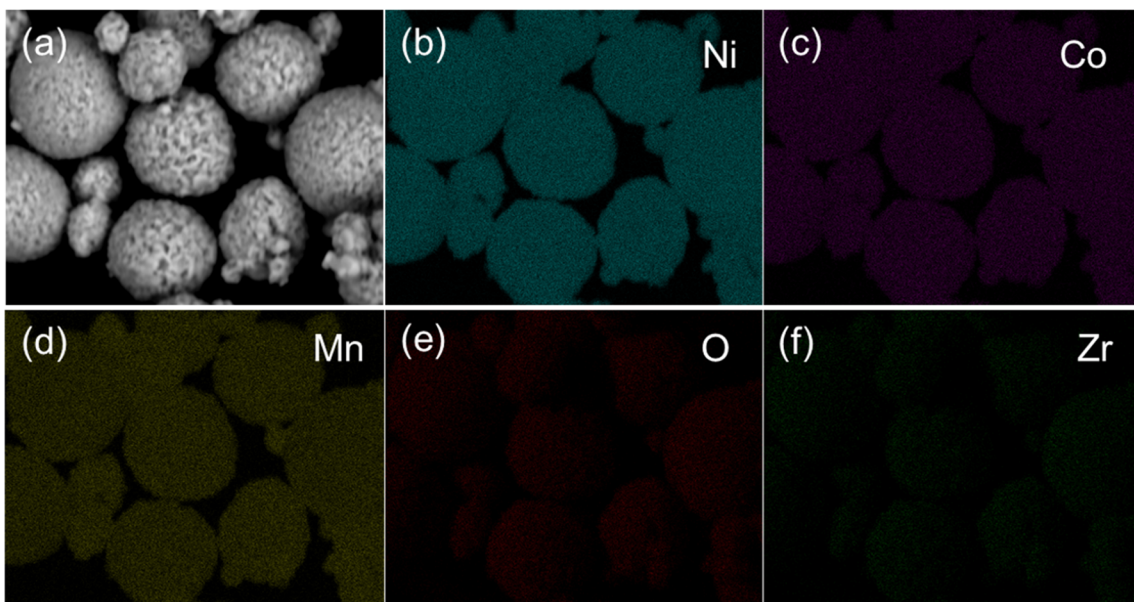
**Fig. 4** EDS mapping of the LZO-NCM cathodes: **a** SEM image of LZO-NCM, and elemental mappings of Ni, Co, Mn, O, and Zr (**b**, **c**, **d**, **e**, **f**)

phenomenon that discharge capacity of the LZO-NCM electrode is lower than that of NCM electrode is probably because the coating layer is electrochemically inactive in the voltage range. With respect to the cycling performance at 1C and 25 °C (Fig. 6b), the LZO-NCM sample exhibits a lower initial discharge capacity (187.4 mAh g^{-1}) than that of the pristine
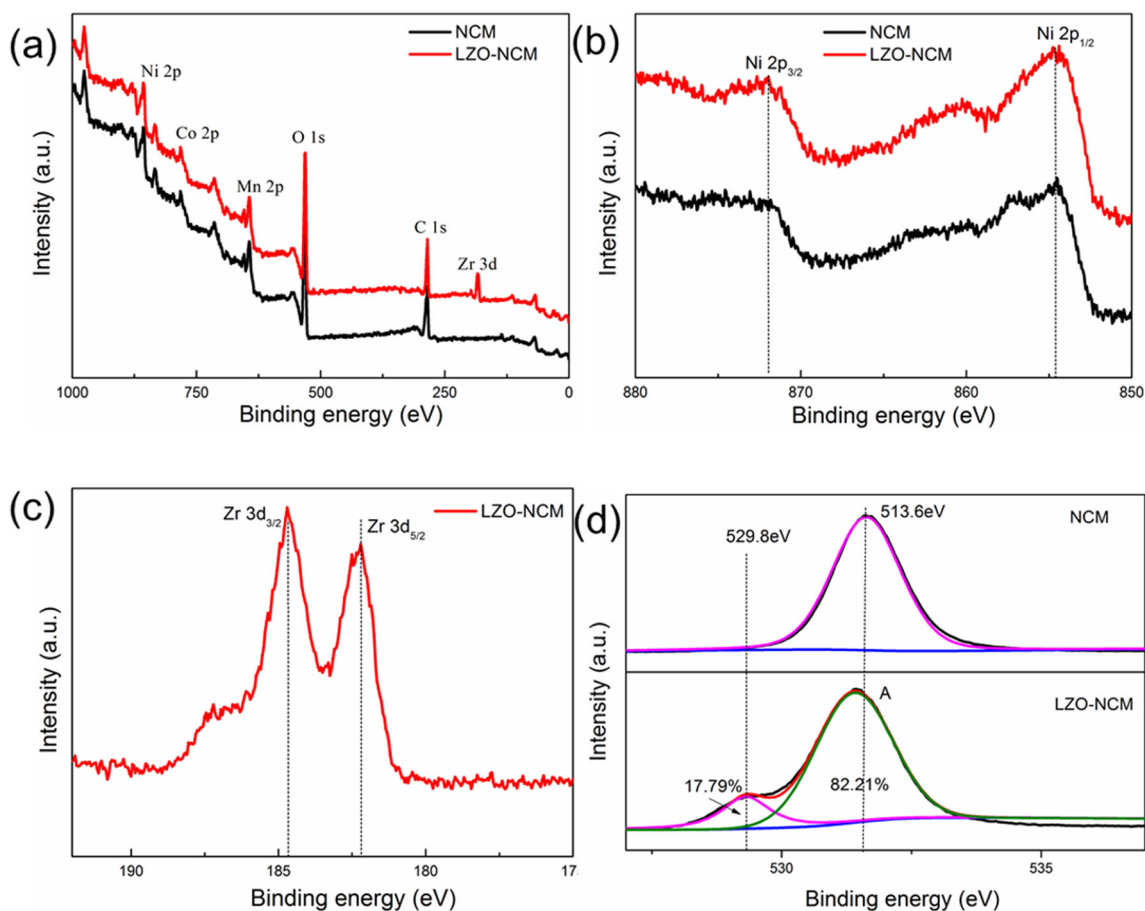
Fig. 5 XPS spectra of **a** full spectra, **b** Ni and **c** Zr, **d** O for NCM and LZO-NCM samples
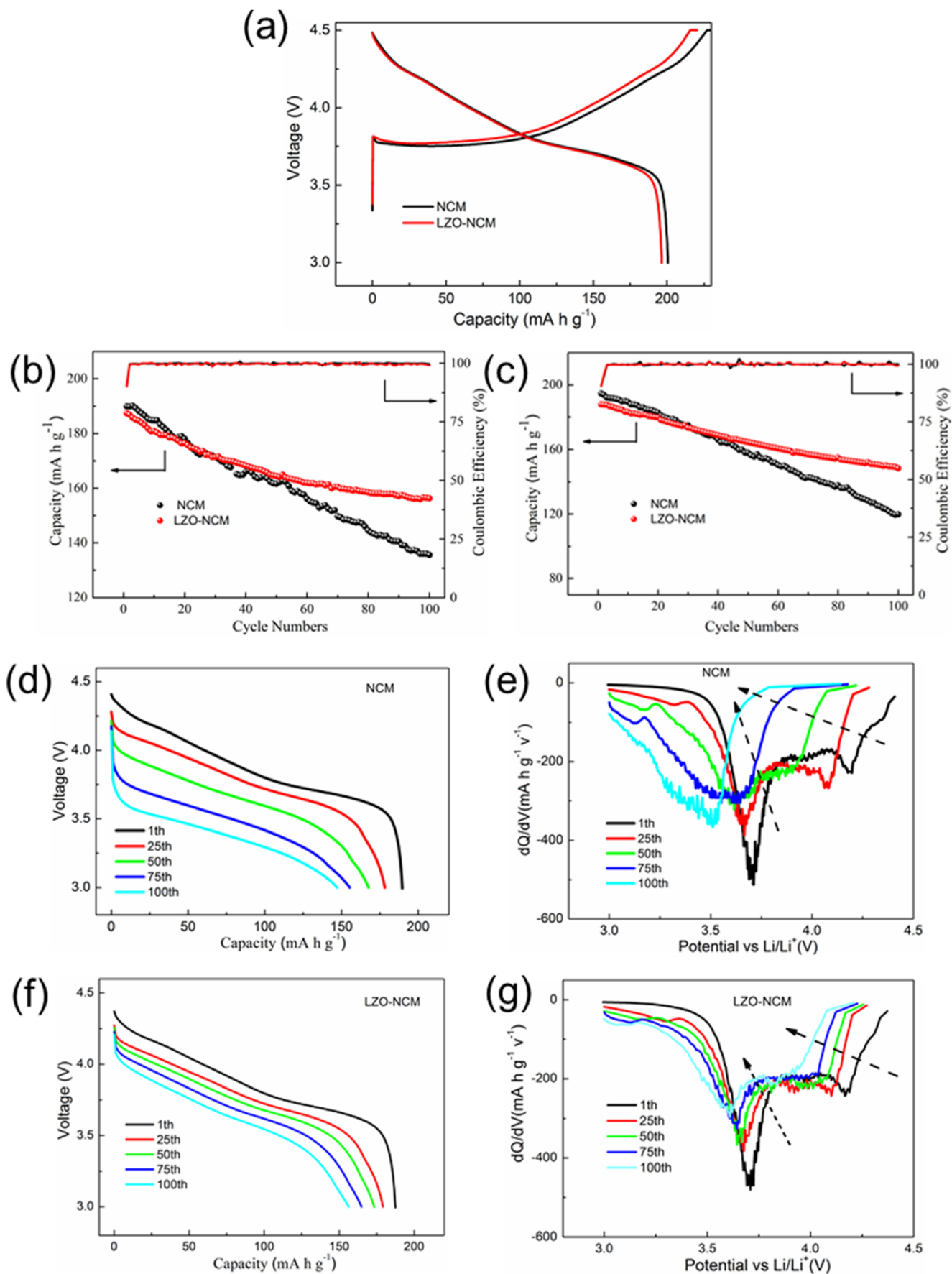
Fig. 6 Electrochemical test of the NCM and LZO-NCM cathodes: **a** charge/discharge curve at 0.1C, **b** 1C cycling performance and coulombic efficiency at 25 °C, **c** 1C cycling performance and coulombic efficiency at 55 °C, **d**, **f** discharge profile at different cycles, **e**, **g** the corresponding dQ/dV profiles

(190.2 mAh g^{-1}). But the LZO-NCM maintains a higher capacity retention (83.4%) than the pristine NCM (71.4%) after 100 cycles. In order to further assess the effectiveness of the LZO coating layer, the cycling performance of 1C rate was tested in a severe condition of 55 °C high temperature. Figure 6c shows the results of this test for the pristine NCM and LZO-NCM electrodes, from which their capacity retentions can be found as 61.5% and 79.0%, respectively. It can be observed that the LZO coating effectively improved the cycle performance of $LiNi_{0.7}Mn_{0.15}Co_{0.15}O_2$, which is consistent with the above analysis.

The discharge curves and corresponding dQ/dV profiles of NCM and LZO-NCM for different cycles at a rate of 1C and 25 °C between 3.0 V and 4.5 V are shown in Fig. 6d–g. Compared with Fig. 6d and f, we can see that LZO-NCM electrode exhibited higher stability for capacity and discharge voltage retention during cycling. Voltage fading and capacity loss resulted from the formation of a spinel-like and rock-like structural framework associated with the relocation of transition metals atomic in the Li layer. Differential capacity analyses were performed to understand the different voltage retention behaviors between NCM and LZO-NCM. From dQ/dV curves (Fig. 6e and g), the peak shift of LZO-NCM is smaller than that of the NCM sample, indicating the suppressed polarizations after LZO coating.

The cyclic voltammograms of the NCM and LZO-NCM after the first and the 50th cycles are shown in Fig. 7a and b. The sharp anodic/cathodic peaks around 3.7 V correspond to the oxidation/reductions of the Ni^{2+}/Ni^{4+} and the small anodic/cathodic peaks around 4.3 V correspond to the structural transformations of hexagonal structures (H2–H3), respectively [42, 43]. The potential differences (ΔE) between the cathodic peak and the anodic peak of NCM after the 1st

**Table 1** The electrochemical impendence fitting results of NCM and LZO-NCM samples

Samples	Cycle number	R_s (Ω)	R_f (Ω)	R_{ct} (Ω)
NCM	1st	3.58	14.94	20.23
	50th	4.91	84.51	824.6
LZO-NCM	1st	7.25	12.45	34.25
	50th	9.05	28.58	185.0

and 50th cycles are 0.074 and 0.206 V, respectively, which are higher than the compared result of LZO-NCM (0.055 and 0.165 V). As in previous reports [11, 44], a smaller ΔE which represents the electrochemical reversibility indicates a smaller reaction polarization. Obviously, the ΔE becomes smaller after LZO coating, indicating that the LZO coating was helpful in improving the electrochemical performance by reducing the electrochemical polarization.

To figure out the origin of positive effect of the LZO coating layer on cycling performance, the EIS for the NCM and LZO-NCM are analyzed and measured after the first and 50th cycles in full charge to 4.5 V state. In Fig. 8a and b, the Nyquist plots of two samples consist of a semicircle in high frequency and a semicircle in middle frequency. According to previous reports, R_s refers to the solution resistance, and R_f represents the surface interface resistance at high-frequency semicircle, while R_{ct} is assigned to the charge transfer resistance at middle-frequency semicircle [45]. Based on the equivalent circuit (Fig. 8c), the calculated resistances are obtained and listed in Table 1. After cycles, the value of R_s in NCM sample was obviously increased while that in LZO-NCM sample basically remained stable. As presented in Table 1, for both samples, their R_{ct} values are upregulated significantly after 50 cycles, but the R_{ct} value of LZO-NCM is remarkably increased from 34.25 to 185.0 Ω after 50 cycles, while that of NCM increased from 20.23 to 824.6 Ω. This result further suggests that the LZO coating might effectively relieve the side reactions between electrolyte and cathode, thereby suppressing the enhancement of the impedance.
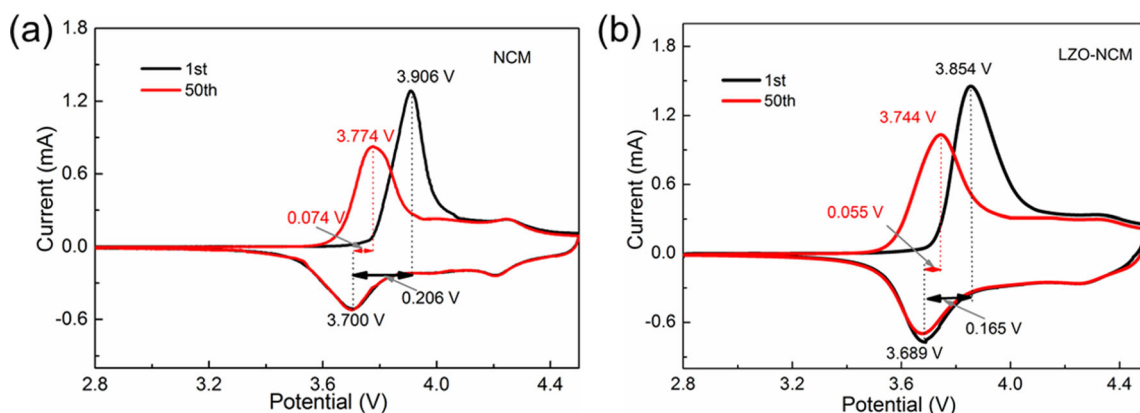

Fig. 7 CV profile of **a** NCM and **b** LZO-NCM at different cycles at a scanning rate of 0.1 mV s^{-1} in a voltage range of 3.0–4.5 V at 25 °C
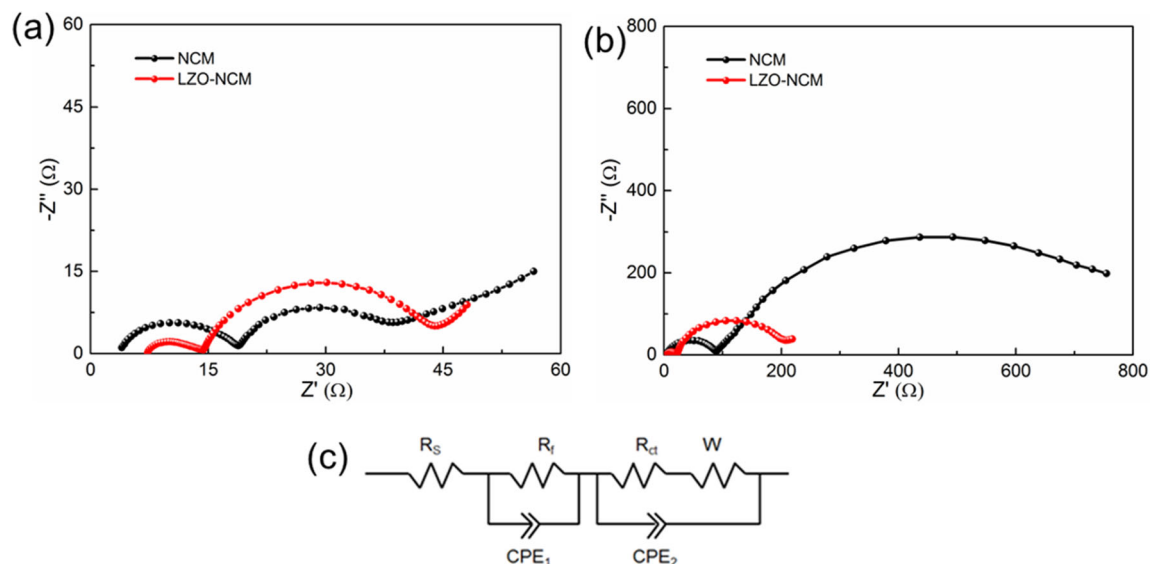
Fig. 8 EIS revealed by Nyquist plots of the NCM and LZO-NCM cathodes, which are analyzed at a rate of 1C after the 1st cycle (**a**) and the 50th cycle (**b**) in a state of full charged to 4.5 V (vs. Li/Li⁺). The corresponding equivalent circuit used for fitting is given in (**c**)

To further explore the reason for improved electrochemical performance of LZO-NCM, high-resolution XPS curves of C 1s, F 1s, and Li 1s of NCM and LZO-NCM electrodes were obtained after 100 cycles. In the C 1s spectra (Fig. 9a), C 1s
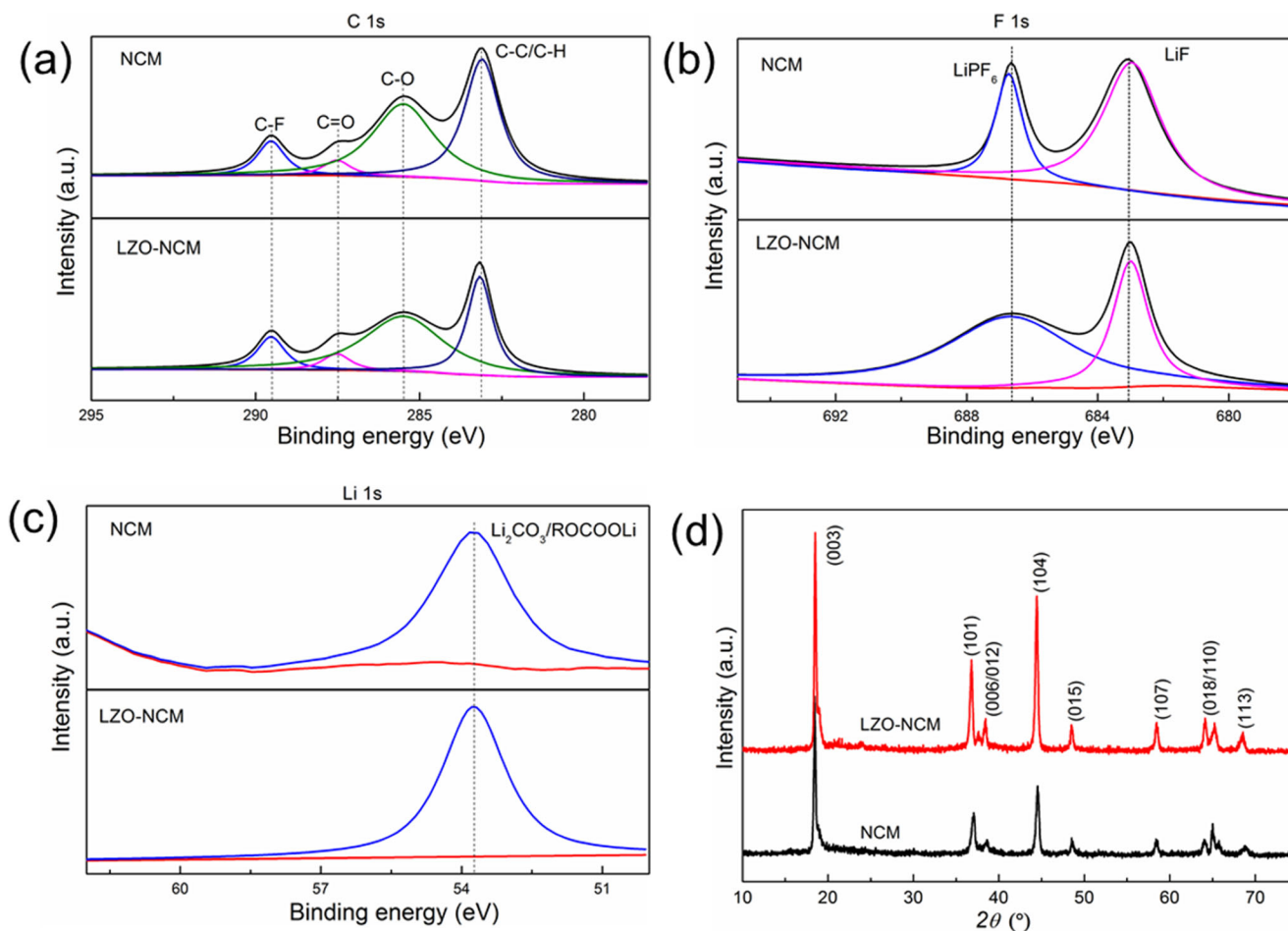
Fig. 9 XPS spectra of **a** C, **b** F, and **c** Li for NCM and LZO-NCM samples after 100 cycles over 3.0–4.5 V; **d** XRD patterns of NCM and LZO-NCM samples after 100 cycles over 3.0–4.5 V

was almost the same at the chemical bond properties expect for intensity. The peak around 683 eV in F 1s spectra is assigned to the LiF which may increase the interface impedance considerably [11]. The peak around 53.8 eV in Li 1s spectra is assigned to the Li_2CO_3/ROCOOLi which mainly originated from the side reactions between electrolyte and cathode [44]. As seen from Fig. 9b and c, the intensity of LiF and Li_2CO_3/ROCOOLi peaks in LZO-NCM are slightly less than those in NCM, indicating that more serious electrolyte decompositions occur on NCM surface. On the contrary, the side reactions can be significantly suppressed by the LZO layer on the NCM particle surface during cycling [46]. As can be seen in Fig. 9d, both electrodes can be indexed to the typical α-$NaFeO_2$ layered structure by the diffraction after 100 cycles, but peak intensities of NCM became weaker than those in the LZO-NCM obviously, which confirm that the LZO coating may effectively strengthen structure of $LiNi_{0.7}Mn_{0.15}Co_{0.15}O_2$ [47].

Conclusions

In summary, a hybrid ZrO_2-Li_2ZrO_3-coated $LiNi_{0.7}Co_{0.15}Mn_{0.15}O_2$ cathode material was successfully achieved by a wet process and systematically investigated. The multifunctional ZrO_2-Li_2ZrO_3 coating layer on NCM surface effectively reduced the side reactions between electrolyte and cathode, thereby significantly optimizing the interfacial structure of electrode and leading to lower impedance increment and enhanced electrochemical stabilities in high cutoff voltage and high temperature. The capacity retention of the $LiNi_{0.7}Co_{0.15}Mn_{0.15}O_2$ cathode was increased from 71.4 to 83.4% by coated ZrO_2-Li_2ZrO_3 after 100 cycles between 3.0 and 4.5 V at 1C and 25 °C. Furthermore, this ZrO_2-Li_2ZrO_3-coated cathode also showed higher capacity retention (79%) than the pristine (61.5%) after 100 cycles at 55 °C. Note that the multifunctional ZrO_2-Li_2ZrO_3 layer can well enhance the electrochemical stabilities of Ni-rich layered oxides. We consider that it should shed some light for the surface design of Ni-rich cathodes with excellent electrochemical performance at high voltages and high temperatures.

References

1. Hu S, Pillai AS, Liang G, Pang WK, Wang H, Li Q, Guo Z (2019) Li-Rich layered oxides and their practical challenges: recent progress and perspectives. Electrochem Energy Rev 2:277–311. https://doi.org/10.1007/s41918-019-00032-8

2. Huang B, Liu D, Qian K, Zhang L, Zhou K, Liu Y, Kang F, Li B (2019) A simple method for the complete performance recovery of degraded Ni-rich $LiNi_{0.70}Co_{0.15}Mn_{0.15}O_2$ cathode via surface reconstruction. ACS Appl Mater Interfaces 11:14076–14084. https://doi.org/10.1021/acsami.8b22529

3. Schipper F, Dixit M, Kovacheva D, Talianker M, Haik O, Grinblat J, Erickson EM, Ghanty C, Major DT, Markovsky B, Aurbach D (2016) Stabilizing nickel-rich layered cathode materials by a high-charge cation doping strategy: zirconium-doped $LiNi_{0.6}Co_{0.2}Mn_{0.2}O_2$. J Mater Chem A 4:16073–16084. https://doi.org/10.1039/c6ta06740a

4. Yang XQ, Tang ZF, Wang HY, Zou BK, Chen CH (2016) Improving the electrochemical performance of $LiNi_{0.5}Co_{0.2}Mn_{0.3}O_2$ by double-layer coating with Li_2TiO_3 for lithium-ion batteries. Ionics (Kiel) 22:2235–2238. https://doi.org/10.1007/s11581-016-1792-0

5. Zeng X, Zhu J, Yang L, Zhou L, Shao L, Hu S, Huang C, Yang C, Qian D, Xi X (2019) Electrochemical stabilities of surface aluminum-doped $LiNi_{0.5}Co_{0.2}Mn_{0.3}O_2$ single crystals under different cutoff voltages. J Electroanal Chem 838:94–100. https://doi.org/10.1016/j.jelechem.2019.02.051

6. Chen Y, Li Y, Li W, Cao G, Tang S, Su Q, Deng S, Guo J (2018) High-voltage electrochemical performance of $LiNi_{0.5}Co_{0.2}Mn_{0.3}O_2$ cathode material via the synergetic modification of the Zr/Ti elements. Electrochim Acta 281:48–59. https://doi.org/10.1016/j.electacta.2018.05.154

7. Dai S, Yuan M, Wang L, Luo L, Chen Q, Xie T, Li Y, Yang Y (2019) Ultrathin-Y_2O_3-coated $LiNi_{0.8}Co_{0.1}Mn_{0.1}O_2$ as cathode materials for Li-ion batteries: synthesis, performance and reversibility. Ceram Int 45:674–680. https://doi.org/10.1016/j.ceramint.2018.09.227

8. Li W, Liu X, Celio H, Smith P, Dolocan A, Chi M, Manthiram A (2018) Mn versus Al in layered oxide cathodes in lithium-ion batteries: a comprehensive evaluation on long-term cyclability. Adv Energy Mater 8:1703154. https://doi.org/10.1002/aenm.201703154

9. Qin C, Cao J, Chen J, Dai GL, Wu TF, Chen Y, Tang YF, Li AD, Chen Y (2016) Improvement of electrochemical performance of nickel rich $LiNi_{0.6}Co_{0.2}Mn_{0.2}O_2$ cathode active material by ultrathin TiO_2 coating. Dalt Trans 45:9669–9675. https://doi.org/10.1039/c6dt01764a

10. Zhang Y, Ren T, Zhang J, Duan J, Li X, Zhou Z, Dong P, Wang D (2019) The role of boracic polyanion substitution on structure and high voltage electrochemical performance of Ni-rich cathode materials for lithium ion batteries. J Alloys Compd 805:1288–1296. https://doi.org/10.1016/j.jallcom.2019.05.090

11. Chen Y, Li Y, Tang S, Lei T, Deng S, Xue L, Cao G, Zhu J (2018) Enhanced electrochemical properties of the Cd-modified $LiNi_{0.6}Co_{0.2}Mn_{0.2}O_2$ cathode materials at high cut-off voltage. J Power Sources 395:403–413. https://doi.org/10.1016/j.jpowsour.2018.05.088

12. Xu Y, Xiang W, Wu ZG et al (2018) Improving cycling performance and rate capability of Ni-rich $LiNi_{0.8}Co_{0.1}Mn_{0.1}O_2$ cathode materials by $Li_4Ti_5O_{12}$ coating. Electrochim Acta 268:358–365. https://doi.org/10.1016/j.electacta.2018.02.049

13. Du R, Bi Y, Yang W et al (2015) Improved cyclic stability of $LiNi_{0.8}Co_{0.1}Mn_{0.1}O_2$ via Ti substitution with a cut-off potential of 4.5 v. Ceram Int 41:7133–7139. https://doi.org/10.1016/j.ceramint.2015.02.026

14. Tornheim A, Trask SE, Zhang Z (2016) Evaluation of electrolyte oxidation stability on charged $LiNi_{0.5}Co_{0.2}Mn_{0.3}O_2$ cathode surface through potentiostatic holds. J Electrochem Soc 163:A1717–A1722. https://doi.org/10.1149/2.1051608jes

15. Dong P, Wang D, Yao Y, Li X, Zhang Y, Ru J, Ren T (2017) Stabilizing interface layer of $LiNi_{0.5}Co_{0.2}Mn_{0.3}O_2$ cathode materials under high voltage using p-toluenesulfonyl isocyanate as film forming additive. J Power Sources 344:111–118. https://doi.org/10.1016/j.jpowsour.2017.01.116

16. Feng Z, Rajagopalan R, Sun D et al (2020) In-situ formation of hybrid Li_3PO_4-$AlPO_4$-$Al(PO_3)_3$ coating layer on $LiNi_{0.8}Co_{0.1}Mn_{0.1}O_2$ cathode with enhanced electrochemical properties for lithium-ion battery. Chem Eng J 382:122959. https://doi.org/10.1016/j.cej.2019.122959

17. Hou P, Li F, Sun Y, Li H, Xu X, Zhai T (2018) Multishell precursors facilitated synthesis of concentration-gradient nickel-rich cathodes for long-life and high-rate lithium-ion batteries. ACS Appl Mater Interfaces 10:24508–24515. https://doi.org/10.1021/acsami.8b06286

18. Wang M, Zhang R, Gong Y, Su Y, Xiang D, Chen L, Chen Y, Luo M, Chu M (2017) Improved electrochemical performance of the $LiNi_{0.8}Co_{0.1}Mn_{0.1}O_2$ material with lithium-ion conductor coating for lithium-ion batteries. Solid State Ionics 312:53–60. https://doi.org/10.1016/j.ssi.2017.10.017

19. Ren T, Zhang J, Wang D, Dong P, Duan J, Li X, Rao S, Huang D, Zhang Y (2018) Enhancing the high-voltage performances of Ni-rich cathode materials by homogeneous La_2O_3 coating via a freeze-drying assisted method. Ceram Int 44:14660–14666. https://doi.org/10.1016/j.ceramint.2018.05.092

20. Gao S, Zhan X, Cheng YT (2019) Structural, electrochemical and Li-ion transport properties of Zr-modified $LiNi_{0.8}Co_{0.1}Mn_{0.1}O_2$ positive electrode materials for Li-ion batteries. J Power Sources 410–411:45–52. https://doi.org/10.1016/j.jpowsour.2018.10.094

21. Li P, Zhao S, Zhuang Y, Adkins J, Zhou Q, Zheng J (2018) Improved electrochemical performance of $LiNi_{0.8}Co_{0.1}Mn_{0.1}O_2$ modified with 4-vinylbenzeneboronic acid. Appl Surf Sci 453:93–100. https://doi.org/10.1016/j.apsusc.2018.05.027

22. Zhang J, Ren T, Duan J, Li X, Dong P, Zhang Y, Wang D (2018) Enhanced high-voltage cycling stability of nickel-rich cathode materials by surface modification using $LaFeO_3$ ionic conductor. JOM 71:1975–1980. https://doi.org/10.1007/s11837-019-03446-3

23. Dong S, Zhou Y, Hai C, Zeng J, Sun Y, Shen Y, Li X, Ren X, Qi G, Zhang X, Ma L (2019) Ultrathin CeO_2 coating for improved cycling and rate performance of Ni-rich layered $LiNi_{0.7}Co_{0.2}Mn_{0.1}O_2$ cathode materials. Ceram Int 45:144–152. https://doi.org/10.1016/j.ceramint.2018.09.145

24. Chen T, Wang F, Li X, Yan X, Wang H, Deng B, Xie Z, Qu M (2019) Dual functional $MgHPO_4$ surface modifier used to repair deteriorated Ni-rich $LiNi_{0.8}Co_{0.15}Al_{0.05}O_2$ cathode material. Appl Surf Sci 465:863–870. https://doi.org/10.1016/j.apsusc.2018.09.250

25. Hu GR, Deng XR, Peng ZD, Du K (2008) Comparison of $AlPO_4$- and $Co_3(PO_4)_2$-coated $LiNi_{0.8}Co_{0.2}O_2$ cathode materials for Li-ion battery. Electrochim Acta 53:2567–2573. https://doi.org/10.1016/j.electacta.2007.10.040

26. Lee DJ, Scrosati B, Sun YK (2011) $Ni_3(PO_4)_2$-coated $Li[Ni_{0.8}Co_{0.15}Al_{0.05}]O_2$ lithium battery electrode with improved cycling performance at 55°C. J Power Sources 196:7742–7746. https://doi.org/10.1016/j.jpowsour.2011.04.007

27. Li X, Zhang K, Wang M, Liu Y, Qu MZ, Zhao W, Zheng J (2018) Dual functions of zirconium modification on improving the electrochemical performance of Ni-rich $LiNi_{0.8}Co_{0.1}Mn_{0.1}O_2$. Sustain Energy Fuels 2:413–421. https://doi.org/10.1039/c7se00513j

28. Huang J, Fang X, Wu Y, Zhou L, Wang Y, Jin Y, Dang W, Wu L, Rong Z, Chen X, Tang X (2018) Enhanced electrochemical performance of $LiNi_{0.8}Co_{0.1}Mn_{0.1}O_2$ by surface modification with lithium-active MoO_3. J Electroanal Chem 823:359–367. https://doi.org/10.1016/j.jelechem.2018.06.035

29. Xu CL, Xiang W, Wu ZG, Li YC, Xu YD, Hua WB, Guo XD, Zhang XB, Zhong BH (2018) A comparative study of crystalline and amorphous $Li_{0.5}La_{0.5}TiO_3$ as surface coating layers to enhance the electrochemical performance of $LiNi_{0.815}Co_{0.15}Al_{0.035}O_2$ cathode. J Alloys Compd 740:428–435. https://doi.org/10.1016/j.jallcom.2017.12.193

30. Zhang Y, Xia G, Zhang J, Wang D, Dong P, Duan J (2020) Boosting high-voltage cyclic stability of nickel-rich layered cathodes in full-cell by metallurgy-inspired coating strategy. Appl Surf Sci 509:145380. https://doi.org/10.1016/j.apsusc.2020.145380

31. Zhang S, Ma J, Hu Z et al (2019) Identifying and addressing critical challenges of high-voltage layered ternary oxide cathode materials. Chem Mater 31:6033–6065. https://doi.org/10.1021/acs.chemmater.9b01557

32. Chen Y, Tang S, Deng S, Lei T, Li Y, Li W, Cao G, Zhu J, Zhang J (2019) Chemical coupling constructs amorphous silica modified $LiNi_{0.6}Co_{0.2}Mn_{0.2}O_2$ cathode materials and its electrochemical performances. J Power Sources 431:8–16. https://doi.org/10.1016/j.jpowsour.2019.05.042

33. Xu Y, Li X, Wang Z, Guo H, Huang B (2015) Structure and electrochemical performance of TiO_2-coated $LiNi_{0.80}Co_{0.15}Al_{0.05}O_2$ cathode material. Mater Lett 143:151–154. https://doi.org/10.1016/j.matlet.2014.12.093

34. Wu F, Zhang X, Zhao T, Li L, Xie M, Chen R (2015) Multifunctional $AlPO_4$ coating for improving electrochemical properties of low-cost $Li[Li_{0.2}Fe_{0.1}Ni_{0.15}Mn_{0.55}]O_2$ cathode materials for lithium-ion batteries. ACS Appl Mater Interfaces 7:3773–3781. https://doi.org/10.1021/am508579r

35. Chen Z, Qin Y, Amine K, Sun YK (2010) Role of surface coating on cathode materials for lithium-ion batteries. J Mater Chem 20:7606. https://doi.org/10.1039/c0jm00154f

36. Liang L, Hu G, Jiang F, Cao Y (2016) Electrochemical behaviours of SiO_2-coated $LiNi_{0.8}Co_{0.1}Mn_{0.1}O_2$ cathode materials by a novel modification method. J Alloys Compd 657:570–581. https://doi.org/10.1016/j.jallcom.2015.10.177

37. Huang Y, Chen J, Ni J, Zhou H, Zhang X (2009) A modified ZrO_2-coating process to improve electrochemical performance of $Li(Ni_{1/3}Co_{1/3}Mn_{1/3})O_2$. J Power Sources 188:538–545. https://doi.org/10.1016/j.jpowsour.2008.12.037

38. Zhan X, Gao S, Cheng YT (2019) Influence of annealing atmosphere on Li_2ZrO_3 –coated $LiNi_{0.6}Co_{0.2}Mn_{0.2}O_2$ and its high-voltage cycling performance. Electrochim Acta 300:36–44. https://doi.org/10.1016/j.electacta.2019.01.077

39. Wang D, Li X, Wang Z, Guo H, Huang Z, Kong L, Ru J (2015) Improved high voltage electrochemical performance of Li_2ZrO_3-coated $LiNi_{0.5}Co_{0.2}Mn_{0.3}O_2$ cathode material. J Alloys Compd 647:612–619. https://doi.org/10.1016/j.jallcom.2015.06.071

40. Kong JZ, Wang SS, Tai GA, Zhu L, Wang LG, Zhai HF, Wu D, Li AD, Li H (2016) Enhanced electrochemical performance of $LiNi_{0.5}Co_{0.2}Mn_{0.3}O_2$ cathode material by ultrathin ZrO_2 coating. J Alloys Compd 657:593–600. https://doi.org/10.1016/j.jallcom.2015.10.187

41. Liu H, Yang Y, Zhang J (2006) Investigation and improvement on the storage property of $LiNi_{0.8}Co_{0.2}O_2$ as a cathode material for lithium-ion batteries. J Power Sources 162:644–650. https://doi.org/10.1016/j.jpowsour.2006.07.028

42. Noh HJ, Youn S, Yoon CS, Sun YK (2013) Comparison of the structural and electrochemical properties of layered $Li[NixCoyMnz]O_2$ (x = 1/3, 0.5, 0.6, 0.7, 0.8 and 0.85) cathode material for lithium-ion batteries. J Power Sources 233:121–130. https://doi.org/10.1016/j.jpowsour.2013.01.063

43. Wu F, Tian J, Su Y, Wang J, Zhang C, Bao L, He T, Li J, Chen S (2015) Effect of Ni^{2+} content on lithium/nickel disorder for Ni-rich cathode materials. ACS Appl Mater Interfaces 7:7702–7708. https://doi.org/10.1021/acsami.5b00645

44. Meng K, Wang Z, Guo H, Li X, Wang D (2016) Improving the cycling performance of $LiNi_{0.8}Co_{0.1}Mn_{0.1}O_2$ by surface coating

with Li$_2$TiO$_3$. Electrochim Acta 211:822–831. https://doi.org/10.1016/j.electacta.2016.06.110

45. Wang L, Zhao J, He X et al (2012) Electrochemical impedance spectroscopy (EIS) study of LiNi$_{1/3}$Co$_{1/3}$Mn$_{1/3}$O$_2$ for Li-ion batteries. Int J Electrochem Sci 7:345–353. https://doi.org/10.1149/2.jes120015

46. Hu SK, Cheng GH, Cheng MY, Hwang BJ, Santhanam R (2009) Cycle life improvement of ZrO$_2$-coated spherical LiNi$_{1/3}$Co$_{1/3}$Mn$_{1/3}$O$_2$ cathode material for lithium ion batteries. J Power Sources 188:564–569. https://doi.org/10.1016/j.jpowsour.2008.11.113

47. Liang H, Wang Z, Guo H, Wang J, Leng J (2017) Improvement in the electrochemical performance of LiNi$_{0.8}$Co$_{0.1}$Mn$_{0.1}$O$_2$ cathode material by Li$_2$ZrO$_3$ coating. Appl Surf Sci 423:1045–1053. https://doi.org/10.1016/j.apsusc.2017.06.283